

Characteristics of flow over traveling wavy foils in a side-by-side arrangement

Gen-Jin Dong and Xi-Yun Lu^{a)}

Department of Modern Mechanics, University of Science and Technology of China, Anhui, Hefei 230026, People's Republic of China

(Received 2 November 2006; accepted 3 April 2007; published online 29 May 2007)

Flow over traveling wavy foils in a side-by-side arrangement has been numerically investigated using the space-time finite element method to solve the two-dimensional incompressible Navier-Stokes equations. The midline of each foil undergoes lateral motion in the form of a streamwise traveling wave, which is similar to the backbone undulation of swimming fish. Based on the phase difference between the adjacent undulating foils, two typical cases, i.e., in-phase and anti-phase traveling wavy movements, are considered in the present study. The effects of lateral interference among the foils on the forces, power consumption, propeller efficiency, and flow structures are analyzed. It is revealed that the lateral interference is of benefit to saving the swimming power in the in-phase case and enhancing the forces in the anti-phase case. Some typical vortex structures, e.g., vortex-pair row, single vortex row, and in-phase and anti-phase synchronized vortex-street, are observed in the wake of the traveling wavy foils. The results obtained in this study provide physical insight into the understanding of hydrodynamics and flow structures for flow over the traveling wavy foils and swimming mechanisms relevant to fish schooling. © 2007 American Institute of Physics. [DOI: 10.1063/1.2736083]

I. INTRODUCTION

There are some explanations for the formation of fish schools. Several reasons have been found and mainly include the following aspects:^{1,2} protection, energy savings or hydrodynamic advantages, social aspects, and foraging. The hydrodynamic aspect of fish schooling is a challenging topic with complex flow phenomena^{1,2} and is desirable to be studied.

To better explore propulsive mechanisms involved in fish swimming, the wave-like swimming motion of the body is usually used as an essential model to deal with the propulsion of fish.³ Since Lighthill⁴ and Wu⁵ first proposed two kinds of mathematical theories for flexible elongated bodies and for flat bodies of large aspect ratio, respectively, further analytical investigations on the inviscid hydromechanics of fish-like propulsion were extensively performed.⁶⁻⁸ On the other hand, experimental studies were carried out to deal with the drag reduction and flow behaviors near the traveling swimming body.^{9,10} In addition, the wake behind the free-swimming fish or organisms were also measured using digital particle image velocimetry to explore the high propulsive efficiencies.¹¹⁻¹³

Viscous flow past traveling wavy bodies has been investigated numerically. Liu *et al.*^{14,15} numerically analyzed the hydrodynamics of an undulatory swimming tadpole and first confirmed that most of the results from the two- and three-dimensional simulations were closely matched with each other. Carling *et al.*¹⁶ used a two-dimensional model combining the dynamics between the creature's movement and the

fluid flow of the surrounding water to deal with a self-propelled swimming movement. Shen *et al.*¹⁷ performed a direct simulation to study the turbulent flow over a flexible wall undergoing a streamwise traveling wave motion and revealed the hydrodynamic behaviors based on drag reduction and optimal propulsive efficiency. The present authors also investigated the hydrodynamics and flow structures around the traveling wavy body to gain an understanding of fish-like swimming mechanisms.^{18,19}

As shown above, extensive studies on the fish-like propulsion of an individual fish swimming alone have been carried out; however, only few early theoretical analyses and experimental observations were performed to deal with hydrodynamic behaviors of fish schooling. Weihs^{20,21} first proposed a model to analyze the inviscid hydromechanics in fish schools under some assumptions, one of which is fish undulating motion in phase. Later, based on the observation of fish schools, Partridge and Pitcher²² reported that neighboring fish should beat their tails in anti-phase and qualitatively analyzed the hydrodynamics. Since then, little further work has been performed on the hydrodynamic function for fish schools. Although some subtle variation in phase from fish to fish may be appropriate in schools, it is believable that the in-phase and anti-phase undulating motions are two typical cases in schools. In addition, the corresponding hydrodynamic behaviors should be significantly different, in particular involving the viscous effect. Since the hydrodynamic behaviors of fish schooling are closely associated with the complex interferences among the fish,^{2,20-22} e.g., streamwise interference and lateral interference, it is reasonable to study them separately to reveal the mechanisms involved in fish schooling.

^{a)} Author to whom correspondence should be addressed. Electronic mail: xlu@ustc.edu.cn

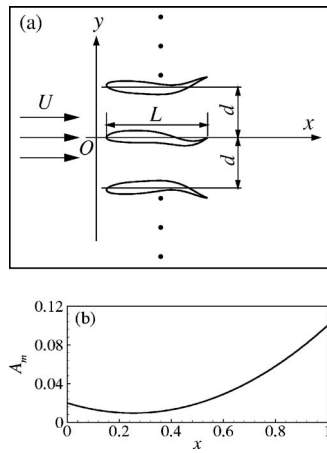


FIG. 1. Schematic of flow configuration: (a) traveling wavy foils in a side-by-side arrangement and (b) distribution of the traveling wave amplitude.

Some work has been performed to investigate the streamwise interference on the mechanisms relevant to fish swimming in vortex wakes. Liao *et al.*^{23,24} and Beal *et al.*²⁵ experimentally found that fish can capture energy from vortices generated in the upstream flow and reduce muscle activity during vortex exploitation with an effective locomotion. Gopalkrishnan *et al.*²⁶ and Streitlien *et al.*²⁷ performed experiments on a flapping foil in vortical flows and found that the foil can exploit the energy for efficient propulsion. In addition, the present authors also carried out a numerical simulation of a foil placed in the wake of a circular cylinder and found that the mean drag force acting on the foil is nearly zero.²⁸

To our knowledge, however, the lateral interference among traveling wavy bodies has never been examined, and therefore it is highly desired to be studied to reveal the flow characteristics. Thus, flow over traveling wavy foils in a side-by-side arrangement has been investigated in the present study. As discussed above, two typical cases, i.e., in-phase and anti-phase traveling wavy movements based on the phase difference between the adjacent undulating foils, are considered. Although we recognize the limitation of this model, we nevertheless feel that the results will be helpful in understanding the relevant mechanisms in fish schooling.

This paper is organized as follows. The physical problem and numerical method are described in Sec. II. The characteristics of flow over a single traveling wavy foil and traveling wavy foils in a side-by-side arrangement are discussed in Sec. III. Finally, concluding remarks are given in Sec. IV.

II. PROBLEM DEFINITION AND NUMERICAL METHOD

A. Physical problem and mathematical formulation

Flow over traveling wavy foils in a side-by-side arrangement is considered. As shown in Fig. 1(a) for the configuration in the frame (x, y) , where x (or x_1) and y (or x_2) are the streamwise and lateral coordinates, respectively, the traveling wavy foils are arranged along the lateral direction. The two-dimensional incompressible Navier-Stokes equations are employed as governing equations. To nondimensionalize the

equations, the chord length of foil L is used as the length scale, and the free-stream velocity U as the velocity scale. The nondimensional equations are then given as

$$\frac{\partial u_i}{\partial x_i} = 0, \quad (1)$$

$$\frac{\partial u_i}{\partial t} + \frac{\partial(u_i u_j)}{\partial x_j} = -\frac{\partial p}{\partial x_i} + \frac{1}{\text{Re}} \frac{\partial^2 u_i}{\partial x_j \partial x_j}, \quad (2)$$

where u_i represents the velocity component in the x_i direction, Re is the Reynolds number defined as $\text{Re} = UL/\nu$ with ν the kinematic viscosity, and p is the pressure normalized by ρU^2 with ρ the fluid density.

In the present study, a NACA0012 airfoil is used as the contour of foil at an equilibrium position of undulating motion. The midline of the i th foil is making a lateral oscillation in the form of a wave traveling in the streamwise direction, described by

$$y_o^i = A_m^i(x) \cos[2\pi(x - c^i t) + \phi^i] + d^i, \quad 0 \leq x \leq 1, \quad (3)$$

where the superscript “ i ” represents the i th foil, A_m^i is the amplitude, c^i is the phase speed, ϕ^i is the phase, and d^i is the lateral position of the midline of foil at an equilibrium position. To model reasonably the lateral motion of the backbone undulation of fish swimming,²⁹ the amplitude $A_m^i(x)$ is approximated by a quadratic polynomial,

$$A_m^i(x) = C_0 + C_1 x + C_2 x^2, \quad (4)$$

where the coefficients C_0 , C_1 , and C_2 are solved from the kinematic data of a steadily swimming saithe,²⁹ which gives $A_m^i(0) = 0.02$, $A_m^i(0.2) = 0.01$, and $A_m^i(1) = 0.10$. The amplitude $A_m^i(x)$ is plotted in Fig. 1(b) and reasonably represents the lateral motion of the backbone undulation of fish swimming. To set the kinematic conditions on the deformable body, as used and confirmed previously by Liu *et al.*^{14,15} and Wassersug and Hoff,³⁰ we assume that the body length is unchanged during traveling wavy and its undulation is purely a lateral compressive motion.

Based on the analysis and observation of fish schools,^{20–22} we consider two typical cases; i.e., in-phase and anti-phase traveling wave motion of the adjacent foils. Thus, in the in-phase case, the phase in Eq. (3) for each foil is chosen as $\phi^i = 0$, while in the anti-phase case, the phases for both the adjacent foils are set as $\phi^i = 0$ and π alternatively. To simplify the problem, we assume that all the traveling wavy foils have the same phase speed ($c = c^i$), amplitude ($A_m = A_m^i$), and lateral equilibrium distance (d) between the adjacent foils.

In the calculation, the computational domain in the lateral direction involves two foils with a width $2d$. Assuming that the number of the foils in a side-by-side arrangement is large enough, periodic boundary conditions are thus employed in the lateral direction. On the surfaces of the traveling wavy foils, no-slip velocity condition is used. Uniform flow is set on the inflow boundary, and the normal and shear stress are specified to be zero at the downstream outflow boundary.

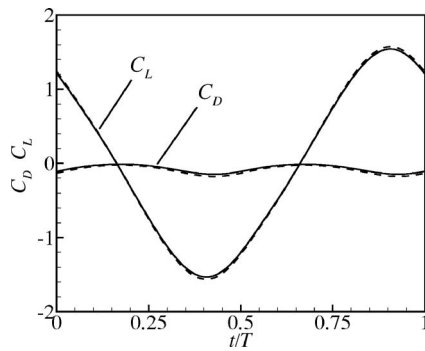


FIG. 2. Time-dependent drag and lateral force coefficients during one cycle for flow over a single traveling wavy foil at $c=2.0$. Solid lines: element number around 2×10^4 , time step 0.005, domain $[-2, 15]$ in the x direction and $[-4, 4]$ in the y direction; dashed lines: element number around 4.8×10^4 , time step 0.0025, domain $[-2, 25]$ in the x direction and $[-6, 6]$ in the y direction.

B. Numerical method

To deal with the flow over arbitrarily deformable bodies, the space-time finite element method³¹ is used based on the streamline-upwind/Petrov-Galerkin and pressure-stabilization/Petrov-Galerkin approaches.³² Equal-in-order basis functions for the velocity and pressure, which are bilinear in space and linear in time, are used, and the Gaussian quadrature is employed for numerical integration. The non-linear equations resulting from the finite-element discretization of the equations are solved by Newton-GMRES (generalized minimal residual) method.³³

In the present study, to adapt the traveling wavy foil, the deformation of mesh is used. The computational domain size is from -2 to 15 in the x direction, and $-0.5d$ to $1.5d$ in the y direction [see Fig. 1(a)]. The element number for each foil is about 2×10^4 and the time step is 0.005.

To confirm the spatial and temporal convergence, we have performed extensive validations. Here, Fig. 2 shows only the time-dependent drag and lateral force coefficients defined below for flow over a single traveling wavy foil at $c=2.0$. Moreover, the corresponding flow structures are also carefully examined. It is found that the results obtained by different element numbers and time steps agree well with each other. Following our numerical tests, we have ensured that the computed results are independent of the time step, grid size (or element number), and computational domain size.

C. Simulation parameters

According to the relevant study on the motion of an aquatic animal at intermediate Reynolds numbers (i.e., $Re \sim 10^3$),³⁴ the Reynolds number is set as 5000 in this study. We start simulations of the viscous flow over a single traveling wavy foil with the phase speed $c=0.5-2.0$. The results of the flow over a single foil can be used as a reference case (denoted by $d=\infty$) for the side-by-side arranged foils. Based on the results, we reasonably choose both typical phase speeds $c=1.5$ and 2.0 employed in the simulations of the flow over the traveling wavy foils in a side-by-side arrangement.

To investigate the effect of lateral interference on the flow characteristics, a variety of lateral distances are examined. After our tests, it is identified that the lateral interference becomes very weak when $d \geq 1$. As the trailing-edge amplitude is 0.1, the lateral distance considered here ranges from $d=0.3$ to 1.0 in the in-phase case and from $d=0.4$ to 1.0 in the anti-phase case.

III. RESULTS

In this section, we present some typical results for the characteristics of flow over a single traveling wavy foil and traveling wavy foils in a side-by-side arrangement. Some typical quantities including the forces, the power consumption, the propeller efficiency and the Strouhal number are analyzed. Moreover, the vortex structures in the wake of the foils are exhibited and several wake patterns are identified. Based on our calculations, periodic variations of time-dependent forces and powers are reached after three to five cycles for all the cases considered here. The time-averaged values used below are obtained over ten cycles in the periodic state.

A. Single traveling wavy foil

1. Forces and power consumption

The drag force acting on the wavy foil and the power needed for it to be propelled are directly relevant to the study of fish locomotion. The total drag force on the wavy foil consists of a friction drag and a form drag due to pressure distribution. Considering an element of the surface along the upper side of the foil $ds = [1 + (dy_w^+/dx)^2]^{1/2} dx$, its tangential direction is $t = (1, dy_w^+/dx) / [1 + (dy_w^+/dx)^2]^{1/2}$, and the wall-normal direction is $n = (-dy_w^+/dx, 1) / [1 + (dy_w^+/dx)^2]^{1/2}$, where y_w^+ represents the lateral position along the upper surface of the foil. The friction force and the pressure force per unit length can then be expressed as^{17,18}

$$\begin{aligned} f_x^f &= \mu \left[-2 \frac{\partial u}{\partial x} \frac{dy_w^+}{dx} + \left(\frac{\partial v}{\partial x} + \frac{\partial u}{\partial y} \right) \right], & f_x^p &= p \frac{dy_w^+}{dx}, \\ f_y^f &= \mu \left[2 \frac{\partial v}{\partial y} - \frac{dy_w^+}{dx} \left(\frac{\partial v}{\partial x} + \frac{\partial u}{\partial y} \right) \right], & f_y^p &= -p, \end{aligned} \quad (5)$$

where u and v represent the velocity components in the x and y directions, respectively, and μ is the kinetic viscosity. Similarly, along the lower surface of the wavy foil, the friction force and the pressure force per unit length can be calculated as well. By performing integration of f_x^f and f_x^p over the foil, the friction force F_F , the pressure force F_P , and the total drag force $F_D = F_F + F_P$ are obtained. The drag coefficients are then defined as, respectively,

$$C_D = \frac{F_D}{\frac{1}{2} \rho U^2 L}, \quad C_{DP} = \frac{F_P}{\frac{1}{2} \rho U^2 L}, \quad C_{DF} = \frac{F_F}{\frac{1}{2} \rho U^2 L}. \quad (6)$$

The total power P_T required for the propulsive motion of the foil consists of two parts.^{17,18} One is the swimming power P_S , required to produce the lateral oscillation of traveling wave motion, and is defined as

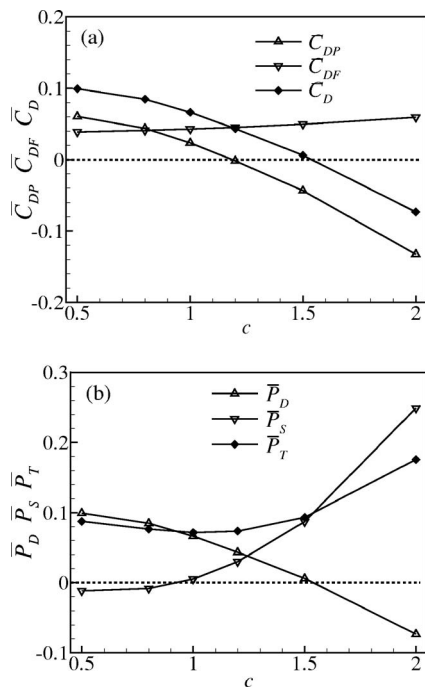


FIG. 3. Time-averaged drag force and power coefficients during one cycle: (a) drag force and (b) power.

$$P_S = - \oint (f_y^p + f_y^f) \frac{dy_w}{dt} ds, \quad (7)$$

where \oint denotes the integration along the foil surface. The other is the power needed to overcome the drag force, and is represented as $P_D = F_D U$. Thus, the total power is obtained by $P_T = P_S + P_D$.

The time-averaged drag force coefficients versus the phase speed c are shown in Fig. 3(a). As c increases, the time-averaged form drag coefficient \bar{C}_{DP} and total drag coefficient \bar{C}_D decrease, and the friction drag coefficient \bar{C}_{DF} increases somewhat. It is noted that \bar{C}_{DP} becomes negative and acts as a thrust force when $c > 1.2$, approximately, and \bar{C}_D becomes negative when $c > 1.5$, approximately, similar to previous findings for viscous flow over a streamwise traveling wavy wall.^{17,18}

The time-averaged powers \bar{P}_T , \bar{P}_S , and \bar{P}_D are shown in Fig. 3(b). As c increases, \bar{P}_S increases and becomes positive for $c > 1$, approximately. The negative value of \bar{P}_S means that the wavy foil motion can be actuated by the flow and that no power input is needed. \bar{P}_D decreases monotonically with c , because of the decrease of \bar{C}_D in Fig. 3(a). When \bar{P}_D is negative, it means that the wavy foil is propelled by the thrust; however, the thrust is at the expense of the swimming power P_S . Thus, \bar{P}_S and \bar{P}_D present the competing mechanisms. The distribution of \bar{P}_T versus c is concave upwards with a minimum around $c = 1.2$, consistent with the optimal performance for propulsion predicted experimentally by the flow over a fish-like swimming body.¹⁰

Considering the undulating body subject to a net thrust (i.e., $\bar{C}_D < 0$), we further introduce the propeller efficiency

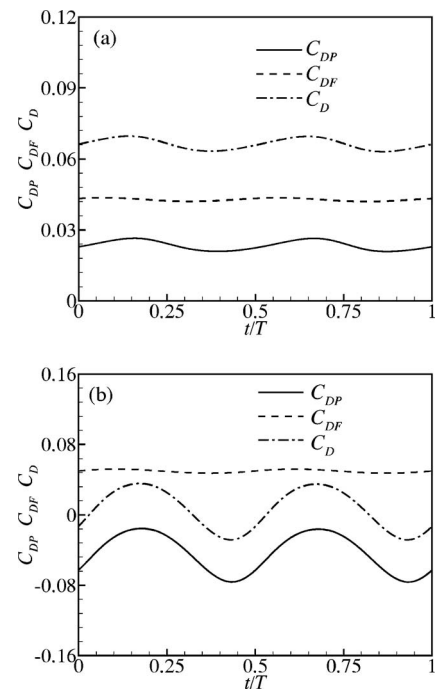


FIG. 4. Time-dependent drag force coefficients during one cycle at $c =$ (a) 1.0 and (b) 1.5.

(or Froude efficiency), as used by Liu *et al.*,^{14,15} defined in a time-averaged manner as the ratio between $-\bar{P}_D$ and \bar{P}_S ; i.e., $\eta = -\bar{P}_D / \bar{P}_S$. Note that for a self-propelled motion, the time-averaged net thrust force is equal to zero, and the propeller efficiency is also zero. Correspondingly, as shown in Fig. 3, the total drag \bar{C}_D is near zero (approximately 5×10^{-3}) at $c = 1.5$, thus, η approaches zero; while a net thrust occurs at $c = 2.0$, η is around 30%.

To elucidate the behavior of time-dependent drag forces, Fig. 4 shows the drag coefficients during one cycle after reaching a periodic state at $c = 1.0$ and 1.5 . The time-dependent friction drag C_{DF} is nearly constant during the cycle. The form drag C_{DP} is always positive at $c = 1.0$ in Fig. 4(a) and negative at $c = 1.5$ in Fig. 4(b). The form drag usually plays an essential role for the propulsion of the traveling wavy foil. To quantitatively show the contribution of pressure distribution on the thrust force, Fig. 5 shows the distributions of $-f_x^p$ defined in Eq. (5) at $t/T = 0$. It is seen that remarkable positive distributions of $-f_x^p$ along both the upper and lower surfaces occur over $0.6 < x < 1.0$ at $c = 1.5$ and 2.0 and contribute a major part to the thrust.

2. Vortex structures in the wake

The vortical wake is closely associated with the hydrodynamic characteristics in fish swimming.³⁵ We further discuss the vortex shedding to understand propulsive performance of the traveling wavy foil. To neatly exhibit the flow patterns, Fig. 6 shows the vorticity contours at only one instant $t/T = 0$. The shear layer is generated along the surface and is gradually shed into the downstream to form concen-

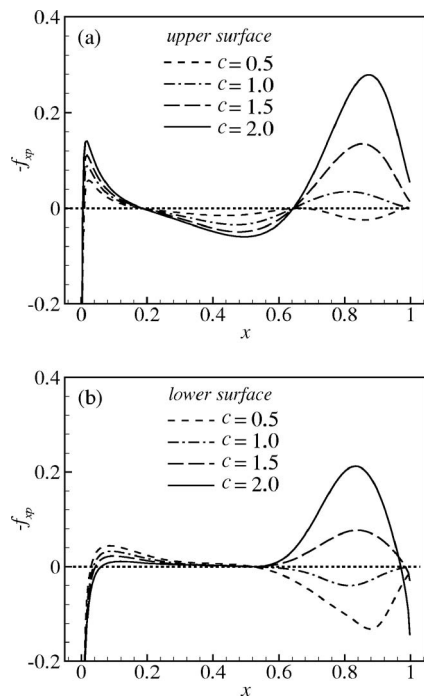


FIG. 5. Distributions of the pressure contribution on the thrust force (i.e., $-f_{sp}^p$) at $t/T=0$ along (a) the upper surface and (b) the lower surface.

trated vortices. There are two vortices with opposite sign shed downstream during one cycle. Finally, a vortex-street occurs in the wake of the foil.

To deal with the influence of the phase speed on the vortex structures, as shown in Fig. 6(a), a similar von Kármán vortex-street is formed at $c=0.8$. As c increases, we carefully identify that the scale of shedding vortex and the lateral width of the vortices array in the near wake decrease gradually, even a vortex-street ranking near as one line at $c=1.2$ in Fig. 6(b). Note that the form drag \bar{C}_{DP} is nearly zero at $c=1.2$ in Fig. 3(a). This behavior is nicely consistent with Wu's theoretical prediction that the vortex-street should rank near as one line for a cruise swimming body (i.e., a zero drag) based on the inviscid flow analysis.³⁶ Further, as c increases, a reverse von Kármán vortex-street occurs in Figs. 6(c) and 6(d). As has been well studied previously,^{19,37} this kind of vortical structure induces a jet-like mean velocity profile in the wake and is of help in generation of the thrust.

Moreover, it is also observed that the vortex-street dissipates quickly for larger c in Fig. 6. We can well understand this phenomenon by means of vorticity dynamics theory. Following vorticity analysis,³⁸ the vorticity dissipation by the viscosity is directly associated with the enstrophy dissipation rate, i.e., $\Phi_{\omega} \equiv \mu \nabla \omega : \nabla \omega$, with ω the vorticity. Therefore, as shown in Fig. 6, when c is higher and wake vortices get closer, the vorticity gradient must become larger, and hence so does the enstrophy dissipation, which is proportional to the square of vorticity gradient (see Φ_{ω}). Further, we examine the square of vorticity gradient (i.e., $|\nabla \omega|^2$ for the two-dimensional flow) in the wake at different instants, and find that the magnitude of $|\nabla \omega|^2$ at $c=2.0$ is higher than that at $c=0.8$ by one order. Thus, it is reasonably predicted that the

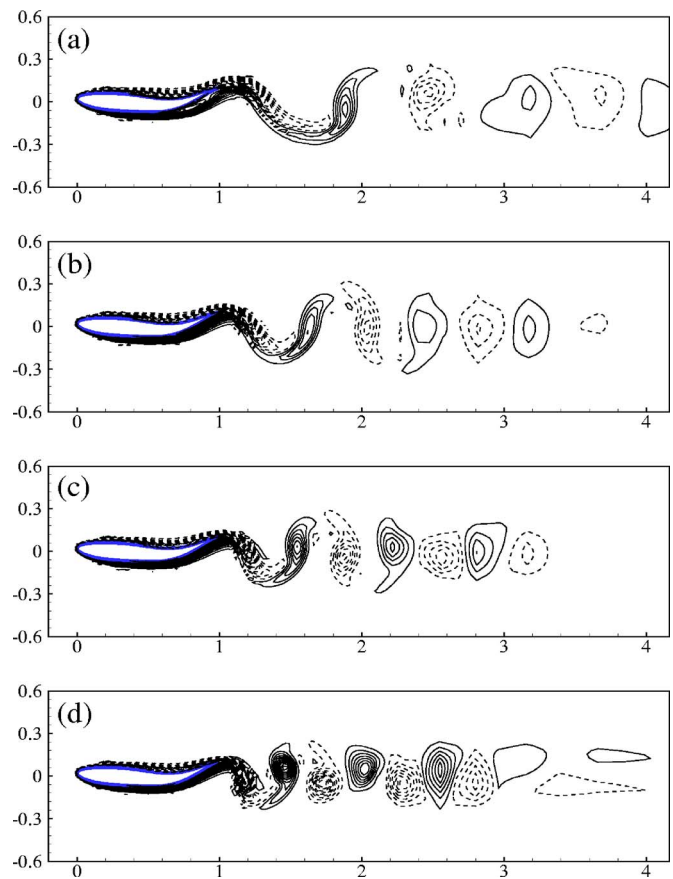


FIG. 6. Vorticity contours for $t/T=0$ at $c=$ (a) 0.8, (b) 1.2, (c) 1.5, and (d) 2.0.

vortex-street can keep its structure up to a long distance in the downstream of the foil at $c=0.8$, and dissipates quickly for larger c ; e.g., $c=2.0$.

We also calculate the Strouhal number (St) for vortices in the wake. The Strouhal number is defined as $St = 2A_m f / U$ with the free-stream velocity (U), the frequency of undulating motion (f), and the width of the wake, taken to be equal to the maximum excursion of the traveling wavy foil's trailing edge ($2A_m$). Similar to fish locomotion,²⁹ a necessary condition for locomotion generation of flow past a traveling wavy body is that the phase speed of the body wave be greater than the forward speed; i.e., $c > 1$.¹⁰ Thus, we can obtain that the Strouhal number is within the interval 0.2–0.4 for $c=1.0$ –2.0 considered here, which lies in the regime naturally selected by swimming and flying animals.³⁹

B. In-phase traveling wavy foils

Based on the understanding of flow characteristics for a single traveling wavy foil, we further deal with the effects of lateral interference among the foils on the hydrodynamics and flow structures. As discussed above, we use $c=1.5$ and 2.0 as two typical phase speeds in the present simulations for the flow over the traveling wavy foils in a side-by-side arrangement. Here, some typical results for the flow over the in-phase traveling wavy foils are shown, and the hydrodynamics and vortex structures in the wake are analyzed.

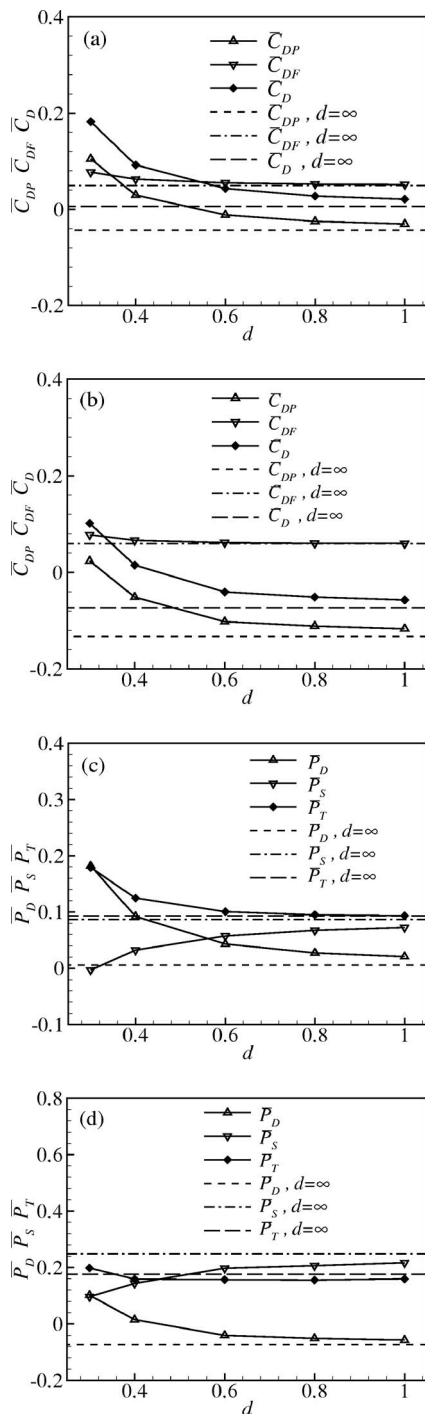


FIG. 7. Time-averaged drag force and power coefficients: (a) drag force at $c=1.5$, (b) drag force at $c=2.0$, (c) power at $c=1.5$, and (d) power at $c=2.0$.

1. Forces and power consumption

The time-averaged drag force coefficients are shown in Figs. 7(a) and 7(b) for $c=1.5$ and 2.0 , respectively. When the lateral distance d between the adjacent foils increases, the drag force coefficients decrease and finally approach to the values for flow over a single foil (henceforth referred to as $d=\infty$). At $d=0.3$, due to the block effect, the foil is subject to a large drag force. The total drag coefficient \bar{C}_D is always positive at $c=1.5$ and becomes negative around $d=0.4$ at

$c=2.0$. We can identify that the lateral interference in the in-phase undulating motion makes against the reduce of drag force.

The distributions of \bar{P}_T , \bar{P}_S , and \bar{P}_D are shown in Figs. 7(c) and 7(d) for $c=1.5$ and 2.0 , respectively. Since \bar{C}_D increases as d decreases, thus \bar{P}_D increases as well. However, it is interesting to find that the swimming power \bar{P}_S decreases as d decreases, and even becomes negative at $d=0.3$ and $c=1.5$. This means that the traveling wavy foils in the in-phase motion can be actuated by the flow without power input when \bar{P}_S is negative. Thus, it is reasonably revealed that the lateral interference is of benefit to saving the swimming power in the in-phase undulating motion.

The main contribution to the total power \bar{P}_T is \bar{P}_D when $d < 0.4$, and exhibits a large power consumption. By carefully examining \bar{P}_T versus d , there exist somewhat different behaviors for $c=1.5$ and 2.0 . At $c=1.5$, \bar{P}_T decreases monotonically and approaches the value at $d=\infty$ as d increases. At $c=2.0$, \bar{P}_T decreases to a minimum value around $d=0.6$ and increases very smoothly to the value at $d=\infty$. It is noted that \bar{P}_T is even less than the value at $d=\infty$ when $d > 0.4$, which may be reasonably ascribed to the saving of swimming power. Further, we show the influence of the lateral interference on the propeller efficiency η . As a typical case for $c=2.0$ in Fig. 7(d), η decreases from 30% at $d=\infty$ to zero at $d=0.4$, approximately, since \bar{C}_D is nearly zero at $d=0.4$ in Fig. 7(b), corresponding to a self-propelled motion of the in-phase traveling wavy foils.

Figure 8 shows the time-dependent drag coefficients during one cycle for several lateral distances at $c=1.5$. The friction drag C_{DF} is nearly constant. Due to the lateral interference, the form drag C_{DP} is always positive during the cycle at $d=0.3$ and 0.4 , becomes alternately positive and negative at $d=0.6$, and negative at $d=0.8$ and 1.0 (not shown here). Similar behaviors are also found for $c=2.0$. Thus, we can obtain that the lateral interference has a notable influence on the time-dependent form drag.

According to the results of the flow over a single wavy foil, it is seen that two peaks of C_D are formed during one cycle in Fig. 4, because two vortices with opposite signs shed into the wake in Fig. 6. We then pay attention on the time-dependent drag force in Fig. 8. It is noted that four local peaks of C_D (or C_{DP}), marked by a black dot (\bullet) in Fig. 8(a) for $d=0.3$, are identified during one cycle. As d increases, the distribution of C_D (or C_{DP}) during one cycle again exhibits two peaks. Thus, it may be reasonably predicted that such different behaviors are associated with not only the pressure distribution over the surface of the foil but also the vortex shedding from the arranged foils, which will be discussed further below.

To exhibit the influence of the lateral interference on the pressure distribution, Fig. 9 shows the instantaneous pressure contours for $t/T=0$ and $c=1.5$. At $d=0.3$ in Fig. 9(a), the pressure varies sharply near the leading and trailing edges of the foils, and is nearly unchanged in the region of $0.15 < x < 0.8$. As d increases, the pressure distribution changes smoothly over the area between the adjacent foils, and the

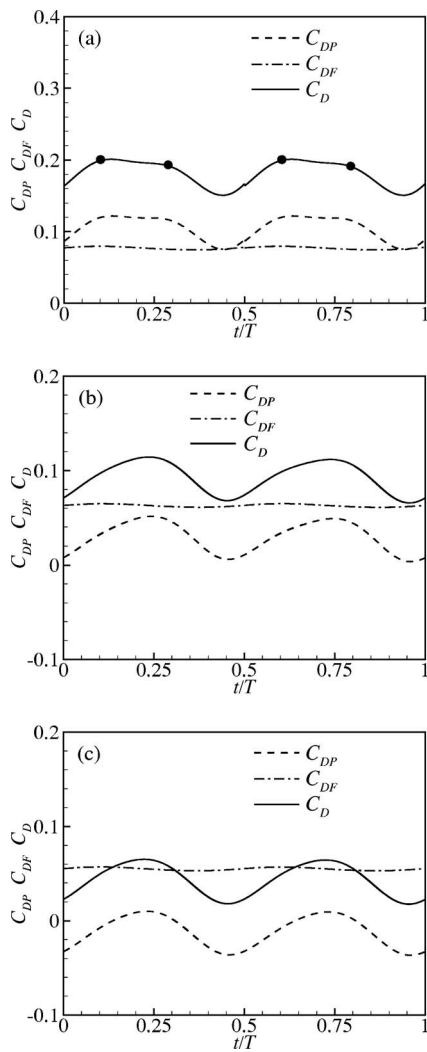


FIG. 8. Time-dependent drag force coefficients during one cycle for $c = 1.5$ at $d =$ (a) 0.3, (b) 0.4, and (c) 0.6.

unchanged pressure region becomes small and disappears around $d \geq 0.6$. Correspondingly, the form drag \bar{C}_{DP} decreases as d increases in Fig. 7(a).

2. Vortex structures in the wake

The vortex shedding in the near wake of the foils is examined. When d is less than the width of the vortex-street formed by the flow over a single foil, as shown in Fig. 6, the lateral interference may play a significant influence on the vortex shedding to form complex vortex structures in the wake. Based on our calculated results, we have identified three kinds of vortex structures in the wake; i.e., vortex-pair row, single vortex row, and in-phase synchronized vortex-street.

Figure 10 shows the vorticity contours at $d=0.3$ and $c = 1.5$. Based on the animation of vortex shedding, we identify that during one cycle, four concentrated vortices, i.e., two positive ones along the lower side of the foil and two negative ones along the upper side of the foil, shed into the wake from each foil, resulting in the four local peaks of C_D in Fig. 8(a). Here, we further describe the time development

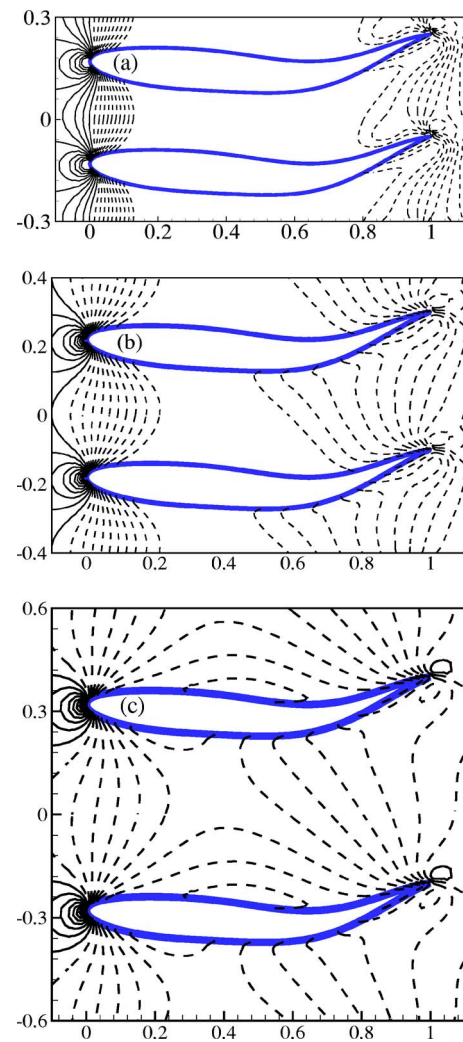


FIG. 9. Instantaneous pressure contours for $c=1.5$ and $t/T=0$ at $d =$ (a) 0.3, (b) 0.4, and (c) 0.6.

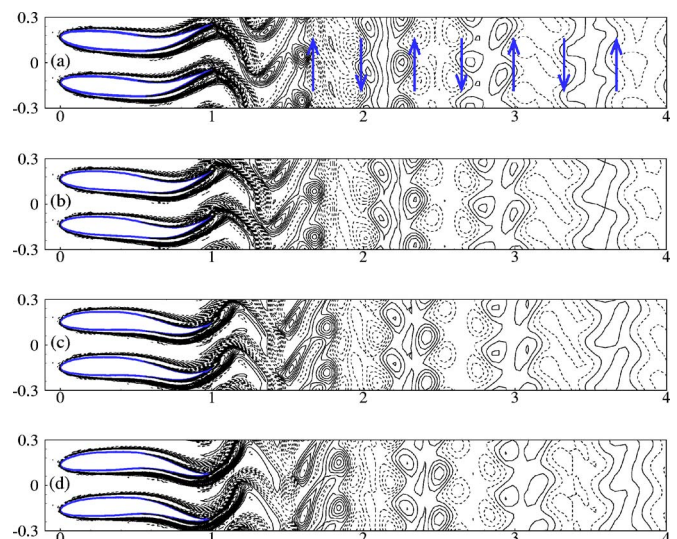


FIG. 10. Vorticity contours for vortex-pair row structures for $d=0.3$ and $c = 1.5$ at $t/T =$ (a) 0/8, (b) 1/8, (c) 2/8, and (d) 3/8. Here, “ \uparrow ” denotes a vortex-pair moving upward and “ \downarrow ” a vortex-pair moving downward.

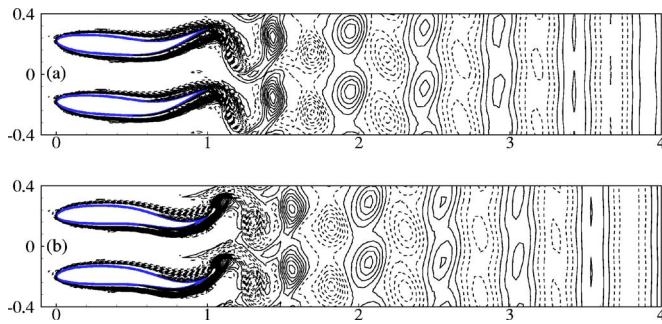


FIG. 11. Vorticity contours for single vortex row structures for $d=0.4$ and $c=1.5$ at $t/T=$ (a) $0/4$ and (b) $1/4$.

of the vortex structures during one cycle. When both the positive vortices are shedding into the wake, we observe that the first positive one is paired with a previous negative vortex to form a vortex-pair that moves upward, marked by “ \uparrow ” in Fig. 10(a), due to their induced velocity, and the second positive one will be paired with a following negative vortex to form another vortex-pair which moves downward, marked by “ \downarrow ” in Fig. 10(a). It is then interesting to note that the vortex-pair rows ranking along the streamwise direction move in the lateral direction with alternately upward and downward motion when they are shedding into the downstream region. Thus, we call the vortex structure a vortex-pair row.

When d increases, as shown in Fig. 11 for $d=0.4$ and $c=1.5$, the vortex structure in the wake becomes a single vortex row. During one cycle, two vortices with opposite signs shed into the wake from each foil. Due to the lateral interference between the vortex-streets shed from the neighboring foils, the vortices with the same sign connect together when they are shedding into the downstream region. Finally, the vortical pattern exhibits the vortex rows with alternately opposite sign ranking along the streamwise direction, i.e., “single vortex row” structure.

When d increases further, the lateral interference becomes weak and the vortex shedding synchronizes from each traveling wavy foil. As is typically shown in Fig. 12 for $d=0.6$ and $c=1.5$, the vortical structure exhibits the vortex-

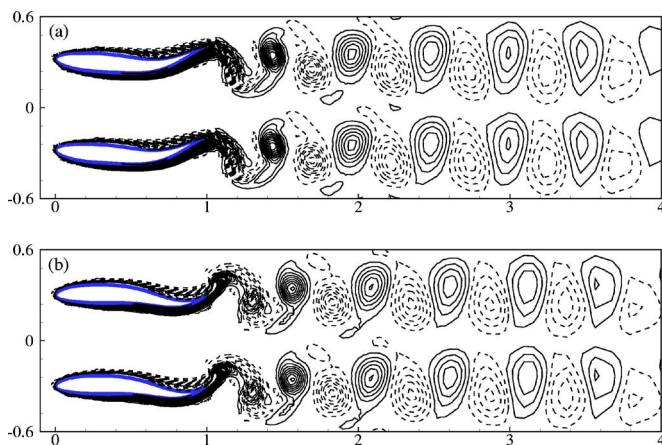


FIG. 12. Vorticity contours for “in-phase synchronized vortex-street” structures for $d=0.6$ and $c=1.5$ at $t/T=$ (a) $0/4$ and (b) $1/4$.

street ranking along the lateral direction and is called the “in-phase synchronized vortex-street.” When $d>0.6$, the vortical structures in the wake are similar to those in Fig. 12.

Following our calculated results, we find that the vortex structures in the wake evolve gradually from the vortex-pair row, to the single vortex row, and further to the in-phase synchronized vortex-street, as d increases. These three kinds of vortex structures are also observed for $c=2.0$. The characteristics of time-dependent forces in Fig. 8 are reasonably consistent with the corresponding vortex structures, which will be further studied based on the derivative-moment transformations in vorticity dynamics.⁴⁰ Moreover, it is observed that, compared with the vortex structures for $d=0.6$ (Fig. 12), the vorticity dissipates somewhat quickly in the wake for $d=0.3$ (Fig. 10). This fact is reasonably associated with the enstrophy dissipation discussed above since the magnitude of $|\nabla\omega|^2$ becomes larger for smaller d .

C. Anti-phase traveling wavy foils

We present some typical results to show the influence of the lateral interference on the forces, power consumption, and vortex structures in the wake for the flow over the anti-phase traveling wavy foils at $c=1.5$ and 2.0 , and discuss different flow characteristics between the in-phase and anti-phase cases.

1. Forces and power consumption

Since the motions of both the adjacent foils are symmetric about their mid-location, we thus exhibit the results for only one foil. The time-averaged drag force coefficients are shown in Figs. 13(a) and 13(b) for $c=1.5$ and 2.0 , respectively. For the flow over a single foil, \bar{C}_D exhibits a small positive value at $c=1.5$ in Fig. 3(a). Due to the lateral interference, \bar{C}_D then becomes larger as d decreases in Fig. 13(a), consistent with an early finding.⁴¹ Similarly, a positive thrust (i.e., $-\bar{C}_D > 0$) occurs at $c=2.0$ in Fig. 3(a); it is seen that the thrust becomes larger as d decreases in Fig. 13(b). A similar argument was also proposed by Weihs,^{20,21} who indicated that the thrust, due to oscillatory movements of the fish school, acting on each individual fish might be increased by tens of percentage points. In Fig. 13(b), the thrust at $d=0.4$ is increased about 30% compared with the value at $d=\infty$. From Fig. 13, it is noticed that the increase of the drag or thrust is mainly contributed by the form drag \bar{C}_{Dp} . Further, based on our extensive calculations for different phase speeds, it is interesting to find that, when the foil is subject to a drag force at $d=\infty$, the foils in the anti-phase arrangement will always undergo a drag force that increases as d decreases; when the foil is subject to a thrust force at $d=\infty$, the foils will always have a thrust force that is enhanced as d decreases.

The distributions of \bar{P}_T , \bar{P}_S , and \bar{P}_D are shown in Figs. 13(c) and 13(d) for $c=1.5$ and 2.0 , respectively. As d decreases, \bar{P}_T increases due to \bar{P}_D for $c=1.5$ and due to P_S for $c=2.0$. Thus, comparing with the results in Fig. 13, it is reasonably found that the lateral interference in the anti-phase case can enhance the drag or thrust force along with a high cost of power consumption. Further, we deal with the

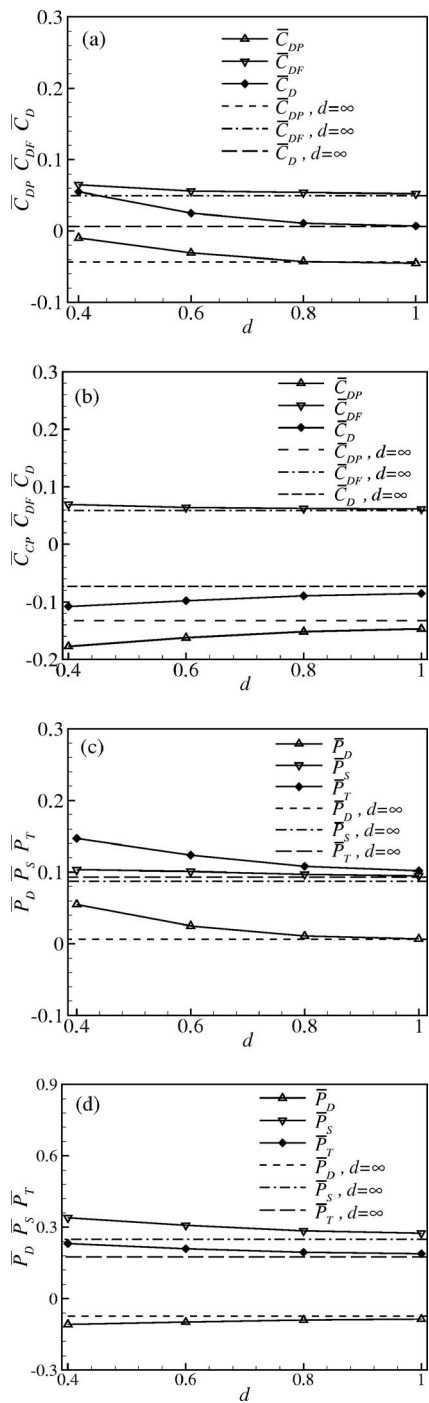


FIG. 13. Time-averaged drag force and power coefficients: (a) drag force at $c=1.5$, (b) drag force at $c=2.0$, (c) power at $c=1.5$, and (d) power at $c=2.0$.

influence of the lateral interference on the propeller efficiency η . As a typical case for $c=2.0$ in Fig. 13(d), η increases somewhat when d decreases, e.g., $\eta=33\%$, approximately, at $d=0.4$, since the thrust is enhanced in the anti-phase arrangement.

2. Vortex structures in the wake

Further, vortex structures in the near wake are examined. Based on our extensive results, as is typically shown in Fig. 14 for the vorticity contours at $c=1.5$ and $t/T=0$, we find

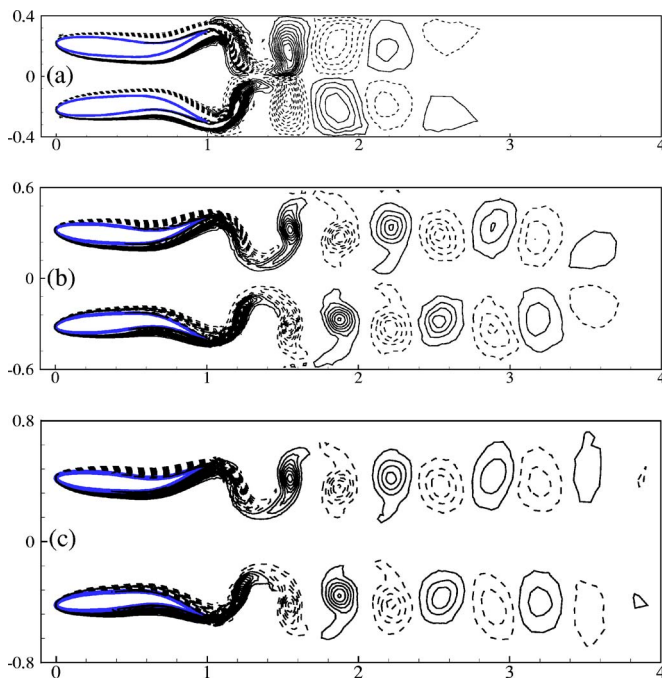


FIG. 14. Vorticity contours for “anti-phase synchronized vortex-street” structures for $c=1.5$ and $t/T=0$ at $d=$ (a) 0.4, (b) 0.6, and (c) 0.8.

only one kind of vortex structure, i.e., anti-phase synchronized vortex-street, which exhibits antisymmetric patterns about the mid-location between the adjacent foils. At $d=0.4$, the vortex-streets shed from the foils are obviously compressed in the lateral direction. When $d>0.6$, the vortex-street from each foil is similar to that at $d=\infty$ in Fig. 6. Meanwhile, the vorticity dissipates somewhat quickly for smaller d due to the enstrophy dissipation effect.³⁸

Based on the vortex structures in the wake of the traveling wavy foils in a side-by-side arrangement, as exhibited in Figs. 12 and 14, two typical vortex structures, i.e., in-phase synchronized and anti-phase synchronized vortex-street, are identified. Similar vortex structures were also found for flow over two stationary cylinders in a side-by-side arrangement.⁴² Comparatively, the other two vortex structures, i.e., the vortex-pair row and single vortex row shown in Figs. 10 and 11, are seldom observed.

IV. CONCLUDING REMARKS

We have investigated flow over traveling wavy foils in a side-by-side arrangement to provide physical insight into the understanding of flow characteristics and swimming mechanisms relevant to fish schooling. The hydrodynamics and flow structures for the flow over the in-phase and anti-phase traveling wavy foils are typically analyzed. Here, we briefly summary the results obtained and discuss the mechanisms relevant to fish schooling.

When the flow is over the in-phase traveling wavy foils, the wavy foils are subject to a large drag force but save the swimming power. These behaviors are nicely consistent with previous findings. Hydrodynamic analysis of fish schooling predicted that the leading-row fish undergo large resistance.^{20,43} From observation and measurement, fish

swimming in close proximity can push off one another and the benefited swimming energy savings occur at a lateral distance of around 0.3 body length.²² In turning maneuvers for fish schooling, the fish prefer the in-phase undulating body motions and may benefit from the swimming power savings as predicted above. Further, we have identified three kinds of vortex structures in the wake, i.e., vortex-pair row, single vortex row, and in-phase synchronized vortex-street, which depend mainly on the lateral distance.

When the flow is over the anti-phase traveling wavy foils, the forces acting on the foils are enhanced, with somewhat expensive power consumption. This behavior is consistent with the fact that the thrust, due to oscillatory movements of the fish school, acting on each individual fish might be increased by tens of percentage points.²² In addition, only one kind of vortex structure, i.e., anti-phase synchronized vortex-street, is observed in the wake of the foils for different lateral distances and phase speeds.

Based on the results obtained in both the in-phase and anti-phase cases, we can understand the relevant mechanisms in fish schooling. Since the in-phase traveling wavy foils (or fish) will induce a strong oscillating flow in their downstream region, compared with the flow in the anti-phase case, the second-row foils (or fish) will undergo a large drag due to the high incidence angle of the local incoming flow.^{21,43} On the other hand, complex vortex structures in the wake are observed in the in-phase case, while only one kind of vortex structure is found in the anti-phase case. Thus, the relative simple downstream flow induced by the anti-phase undulating motion will be helpful for the fish to keep the benefited array pattern in fish schooling. Thus, similar to previous analysis and observation,²² it is reasonably predicted that the fish swimming in schools may be likely to perform the anti-phase undulating body motions. In fish turning maneuvers in schools, the fish may prefer to make the in-phase undulating body motions for swimming energy savings.

The results obtained in this study are helpful to understand hydrodynamics and flow structures for the flow over the traveling wavy foils and the relevant swimming mechanisms of fish schooling. However, the flow characteristics in fish schooling are certainly far more complex and diverse than the simple model considered here. Ideally, three-dimensional computation around flexible bodies is desirable and is a target in our further work.

ACKNOWLEDGMENTS

This work was supported by the National Natural Science Foundation of China (Contract No. 10332040), the Innovation Project of the Chinese Academy of Sciences (Contract No. KJCX-SW-L04), the Program of Hundred-Talent of the Chinese Academy of Sciences, and the Program for Changjiang Scholars and Innovative Research Team in University. The authors thank Professor L.-X. Zhuang and Professor J.-Z. Wu for their valuable comments.

¹J. K. Parrish and L. E. Keshet, "Complexity, pattern and evolutionary trade-offs in animal aggregation," *Science* **284**, 99 (1999).

²S. Stöcker, "Models for tuna school formation," *Math. Biosci.* **156**, 167 (1999).

- ³M. S. Triantafyllou, G. S. Triantafyllou, and D. K. P. Yue, "Hydrodynamics of fishlike swimming," *Annu. Rev. Fluid Mech.* **32**, 33 (2000).
- ⁴M. J. Lighthill, "Note on the swimming of slender fish," *J. Fluid Mech.* **9**, 305 (1960).
- ⁵T. Y. Wu, "Swimming of a waving plate," *J. Fluid Mech.* **10**, 321 (1961).
- ⁶M. G. Chopra and T. Kambe, "Hydromechanics of lunata-tail swimming propulsion," *J. Fluid Mech.* **79**, 49 (1977).
- ⁷J. Y. Cheng, L. X. Zhuang, and B. G. Tong, "Analysis of swimming of three-dimensional waving plates," *J. Fluid Mech.* **232**, 341 (1991).
- ⁸Q. Zhu, M. J. Wolfgang, D. K. P. Yue, and M. S. Triantafyllou, "Three-dimensional flow structures and vorticity control in fish-like swimming," *J. Fluid Mech.* **468**, 1 (2002).
- ⁹M. Wolfgang, J. M. Anderson, M. A. Grosenbaugh, D. K. P. Yue, and M. S. Triantafyllou, "Nearbody flow dynamics in swimming fish," *J. Exp. Biol.* **202**, 2303 (1999).
- ¹⁰D. S. Barrett, M. S. Triantafyllou, D. K. P. Yue, M. A. Grosenbaugh MA, and M. Wolfgang, "Drag reduction in fish-like locomotion," *J. Fluid Mech.* **392**, 183 (1999).
- ¹¹E. Stamhuis and J. Videler, "Quantitative flow analysis around aquatic animals using laser sheet particle image velocimetry," *J. Exp. Biol.* **198**, 283 (1995).
- ¹²E. Drucker and G. Lauder, "Locomotor forces on a swimming fish: three-dimensional vortex wake dynamics quantified using digital particle image velocimetry," *J. Exp. Biol.* **202**, 2393 (1999).
- ¹³C. D. Wilga and G. V. Lauder, "Hydrodynamic function of the shark's tail," *Nature (London)* **430**, 850 (2004).
- ¹⁴H. Liu, R. Wassenberg, and K. Kawachi, "A computational fluid dynamics study of tadpole swimming," *J. Exp. Biol.* **199**, 1245 (1996).
- ¹⁵H. Liu, R. Wassenberg, and K. Kawachi, "The three-dimensional hydrodynamics of tadpole swimming," *J. Exp. Biol.* **200**, 2807 (1997).
- ¹⁶J. Carling, T. L. Williams, and G. Bowtell, "Self-propelled anguilliform swimming: simultaneous solution of the two-dimensional Navier-Stokes equations and Newton's laws of motion," *J. Exp. Biol.* **201**, 3143 (1998).
- ¹⁷L. Shen, X. Zhang, D. K. P. Yue, and M. S. Triantafyllou, "Turbulent flow over a flexible wall undergoing a streamwise travelling wave motion," *J. Fluid Mech.* **484**, 197 (2003).
- ¹⁸G. J. Dong and X. Y. Lu, "Numerical analysis on the propulsive performance and vortex shedding of fish-like travelling wavy plate," *Int. J. Numer. Methods Fluids* **48**, 1351 (2005).
- ¹⁹J. Z. Wu, Z. L. Pan, and X. Y. Lu, "Unsteady fluid-dynamic force solely in terms of control-surface integral," *Phys. Fluids* **17**, 098102 (2005).
- ²⁰D. Weihs, "Hydromechanics of fish schooling," *Nature (London)* **241**, 290 (1973).
- ²¹D. Weihs, "Some hydrodynamical aspects of fish schooling," *Swimming Flying Nature* **2**, 703 (1975).
- ²²B. L. Partridge and T. J. Pitcher, "Evidence against a hydrodynamic function for fish schools," *Nature (London)* **279**, 418 (1979).
- ²³J. C. Liao, D. N. Beal, G. V. Lauder, and M. S. Triantafyllou, "The Kármán gait: novel body kinematics of rainbow trout swimming in a vortex street," *J. Exp. Biol.* **206**, 1059 (2003).
- ²⁴J. C. Liao, D. N. Beal, G. V. Lauder, and M. S. Triantafyllou, "Fish exploiting vortices decrease muscle activity," *Science* **302**, 1566 (2003).
- ²⁵D. N. Beal, F. S. Hower, M. S. Triantafyllou, J. C. Liao, and G. V. Lauder, "Passive propulsion in vortex wakes," *J. Fluid Mech.* **549**, 385 (2006).
- ²⁶R. Gopalkrishnan, M. S. Triantafyllou, G. S. Triantafyllou, and D. Barrett, "Active vorticity control in a shear flow using a flapping foil," *J. Fluid Mech.* **274**, 1 (1994).
- ²⁷K. Streitlien, G. S. Triantafyllou, and M. S. Triantafyllou, "Efficient foil propulsion through vortex control," *AIAA J.* **34**, 2315 (1996).
- ²⁸Q. Liao, G. J. Dong, and X. Y. Lu, "Vortex formation and force characteristics of a foil in the wake of a circular cylinder," *J. Fluids Struct.* **19**, 491 (2004).
- ²⁹J. J. Videler, *Fish Swimming* (Chapman & Hall, London, 1993).
- ³⁰R. Wassersug and K. Hoff, "The kinematics of swimming in anuran larvae," *J. Exp. Biol.* **119**, 1 (1985).
- ³¹T. E. Tezduyar, M. Behr, and J. Liou, "A new strategy for finite element computation involving moving boundaries and interfaces—The deforming-spatial-domain/space-time procedure: I. The concept and the preliminary numerical tests," *Comput. Methods Appl. Mech. Eng.* **94**, 339 (1992).
- ³²T. E. Tezduyar, S. Mittal, S. E. Ray, and R. Shin, "Incompressible flow computations with bilinear and linear equal-order-interpolation velocity-pressure elements," *Comput. Methods Appl. Mech. Eng.* **95**, 221 (1992).
- ³³Y. Saad and M. Schultz, "GMRES: A generalized minimal residual algo-

- rithm for solving nonsymmetric linear systems,” SIAM (Soc. Ind. Appl. Math.) J. Sci. Stat. Comput. **7**, 856 (1986).
- ³⁴M. J. McHenry, E. Azizi, and J. A. Strother, “The hydrodynamics of locomotion at intermediate Reynolds numbers: undulatory swimming in ascidian larvae (*Botrylloides* sp.),” J. Exp. Biol. **206**, 327 (2003).
- ³⁵G. V. Lauder, “Function of the caudal fin during locomotion in fishes: Kinematics, flow visualization, and evolutionary patterns,” Am. Zool. **40**, 101 (2000).
- ³⁶T. Y. Wu, “On theoretical modeling of aquatic and aerial animal locomotion,” Adv. Appl. Mech. **38**, 291 (2001).
- ³⁷X. Y. Lu and Q. Liao, “Dynamic responses of a two-dimensional flapping foil motion,” Phys. Fluids **18**, 098104 (2006).
- ³⁸J. Z. Wu, H. Y. Ma, and M. D. Zhou, *Vorticity and Vortex Dynamics* (Springer-Verlag, Berlin, 2006).
- ³⁹G. Taylor, R. Nudds, and A. Thomas, “Flying and swimming animals cruise at a Strouhal number tuned for high power efficiency,” Nature (London) **425**, 707 (2003).
- ⁴⁰J. Z. Wu, X. Y. Lu, and L. X. Zhuang, “Integral force acting on a body due to local flow structures,” J. Fluid Mech. **576**, 265 (2007).
- ⁴¹L. Rosenhead, “Vortex dynamics analysis of unsteady vortex wakes,” Philos. Trans. R. Soc. London, Ser. A **228**, 275 (1928).
- ⁴²S. Kang, “Characteristics of flow over two circular cylinders in a side-by-side arrangement at low Reynolds numbers,” Phys. Fluids **15**, 2486 (2003).
- ⁴³D. Weihs, “A hydromechanical analysis of fish turning manoeuvres,” Proc. R. Soc. London, Ser. B **182**, 59 (1972).